Mechanism of the Reaction Catalyzed by Mandelate Racemase. 2. Crystal Structure of Mandelate Racemase at 2.5-Å Resolution: Identification of the Active Site and Possible Catalytic Residues[†,‡]

David J. Neidhart,[*,§] P. Lynne Howell,[∥] and Gregory A. Petsko[*,⊥]
Department of Chemistry, Massachusetts Institute of Technology, Cambridge, Massachusetts 02139
Vincent M. Powers,[#] Rongshi Li,[▽] and George L. Kenyon
Department of Pharmaceutical Chemistry, University of California, San Francisco, California 94143
John A. Gerlt
Department of Chemistry and Biochemistry, University of Maryland, College Park, Maryland 20742
Received April 4, 1991; Revised Manuscript Received June 14, 1991

ABSTRACT: The crystal structure of mandelate racemase (MR) has been solved at 3.0-Å resolution by multiple isomorphous replacement and subsequently refined against X-ray diffraction data to 2.5-Å resolution by use of both molecular dynamics refinement (XPLOR) and restrained least-squares refinement (PROLSQ). The current crystallographic *R*-factor for this structure is 18.3%. MR is composed of two major structural domains and a third, smaller, C-terminal domain. The N-terminal domain has an $\alpha + \beta$ topology consisting of a three-stranded antiparallel β-sheet followed by an antiparallel four α-helix bundle. The central domain is a singly wound parallel α/β-barrel composed of eight central strands of β-sheet and seven α-helices. The C-terminal domain consists of an irregular L-shaped loop with several short sections of antiparallel β-sheet and two short α-helices. This C-terminal domain partially covers the junction between the major domains and occupies a region of the central domain that is filled by an eighth α-helix in all other known parallel α/β-barrels except for the barrel domain in muconate lactonizing enzyme (MLE) [Goldman, A., Ollis, D. L., & Steitz, T. A. (1987) *J. Mol. Biol. 194*, 143] whose overall polypeptide fold and amino acid sequence are strikingly similar to those of MR [Neidhart, D. J., Kenyon, G. L., Gerlt, J. A., & Petsko, G. A. (1990) *Nature 347*, 692]. In addition, the crystal structure reveals that, like MLE, MR is tightly packed as an octamer of identical subunits. The active site of MR is located between the two major domains, at the C-terminal ends of the β-strands in the α/β-barrel domain. The catalytically essential divalent metal ion is ligated by three side-chain carboxyl groups contributed by residues of the central β-sheet. A model of a productive substrate complex of MR has been constructed on the basis of difference Fourier analysis at 3.5-Å resolution of a complex between MR and (*R,S*)-*p*-iodomandelate, permitting identification of residues that may participate in substrate binding and catalysis. The ionizable groups of both Lys 166 and His 297 are positioned to interact with the chiral center of substrate, suggesting that both of these residues may function as acid/base catalysts. The results of these structural studies support the conclusions reached from the chemical and kinetic experiments described in the preceding paper regarding the number and chemical properties of the bases in the active site of MR [Powers, V. M., Koo, C., Kenyon, G. K., Gerlt, J. A., & Kozarich, J. W. (1991) *Biochemistry* (first paper of three in this issue)]. This is the first three-dimensional structure of a racemase to be determined.

The studies described in the previous paper (Powers et al., 1991) provided chemical and kinetic evidence that the mechanism of the reaction catalyzed by mandelate racemase (MR)[1] involves two acid/base catalysts, one to abstract a proton from the α-carbon to generate a putative intermediate that has at least partial resonance-stabilized carbanionic character[2] and the second to protonate the intermediate on the opposite face to accomplish the inversion of configuration of the chiral center. On the basis of the observed exchange

[†] This research was supported in part by Grants GM-40570 (J.A.G., G.L.K., and G.A.P.), AR-17323 (G.L.K.), and GM-26788 (G.A.P.) from the National Institutes of Health. This is paper 14 in a series on mandelate racemase; paper 13 is Powers et al. (1991).

[‡] Crystallographic coordinates have been deposited with the Brookhaven Protein Data Bank.

[§] Present address: Laboratory for Protein Crystallography, Department 47E, Abbott Laboratories, Abbott Park, IL 60064.

[∥] Present address: Institute Pasteur, Paris, France.

[⊥] Present address: Rosenstiel Basic Medical Sciences Research Center, Brandeis University, Waltham, MA 02254.

[#] Present address: Department of Molecular and Cell Biology, University of California, Berkeley, CA, 94720.

[▽] Present address: College of Pharmacy, Dalhousie University, Halifax, Nova Scotia B3H3J5, Canada.

[1] Abbreviations: DTNB, 5,5′-dithiobis(2-nitrobenzoic acid); F^+, F^-, structure factor magnitudes with opposite anomalous scattering contributions; F_o, F_c, observed and calculated structure factors, respectively; F_P, F_{PH}, structure factor magnitudes for native protein and for protein plus heavy atom, respectively; MIR, multiple isomorphous replacement; MLE, muconate lactonizing enzyme; MR, mandelate racemase; PIP, bis(μ-iodo)bis(ethylenediamine)diplatinum(II) nitrate; *R*-factor, = $(\sum|F_o - F_c|)/\sum F_o$; SAS, single anomalous scattering; SDS–PAGE, sodium dodecyl sulfate–polyacrylamide gel electrophoresis; SIR, single isomorphous replacement; SIRSAS, single isomorphous replacement with anomalous scattering.

[2] Whether the intermediate is an enolate anion (carbanion) derived by abstraction of a proton from mandelate anion or a charge-neutralized mandelate anion (protonated or metal ion coordinated) or an enol that could be obtained by protonation of an enolate anion is presently unknown. While this distinction is mechanistically important, the studies described in this and the preceding and following papers (Powers et al., 1991; Landro et al., 1991) address only the number and identities of the active site bases that are involved in forming the putative intermediate and not the extent of charge neutralization of the intermediate. Accordingly, the product of proton abstraction from mandelate by an active site base will be referred to as the "intermediate".

0006-2960/91/0430-9264$02.50/0

Table I: Diffraction Data on Mandelate Racemase Crystals[a]

crystal	resolution range (Å)	cell dimensions (Å)			no. > 2σ	no. total	R_{sym}[b] (I)	R_{merge}[c] (I)
		a	b	c				
native 1	∞–5.0	125.1	125.1	106.3	1653	1990		
native 2	5.2–3.5	124.5	124.5	106.1	3018	3755		
native 3	3.55–2.5	124.7	124.5	106.4	4799	9494		6.4
Eu 1	∞–5.0	124.5	124.7	106.4	3288	3952	3.4	
Eu 2	5.2–3.5	124.4	124.4	106.1	5910	7504	4.9	
Eu 3	3.55–3.0	124.5	124.5	106.1	3950	6738	8.5	6.7
Pt	∞–4.0	124.6	124.6	106.2	4694	5735	3.0[d]	
PIP 1	∞–4.35	124.4	124.4	106.2	3933	4797	3.5	
PIP 2	4.45–3.5	124.5	124.6	106.2	2167	2818		5.1
Hg 1	∞–5.0	124.5	124.4	106.0	2940	3960	4.3	
Hg 2	5.1–3.5	124.6	124.6	105.6	2550	3654		
Hg 3	3.55–3.0	124.6	124.7	106.0	1679	3369		6.5

[a] All data were collected with use of a Nicolet P3 diffractometer with a sealed tube source. Full-width ω scans were recorded with separate background measurements for each reflection. [b] R_{sym} is defined for Friedel pairs measured from centric zones of derivatives. [c] R_{merge} is the merging R-factor for overlapping reflections between all crystals used to collect a data set. [d] Freidel pairs measured to 5.0-Å resolution.

of solvent hydrogen into remaining substrate, the conjugate acid of the (*S*)-specific base was deduced to be polyprotic since in D_2O solvent deuterium was efficiently incorporated into substrate (*S*)-mandelate whereas the conjugate acid of the (*R*)-specific base was deduced to be monoprotic since solvent deuterium was not incorporated into substrate (*R*)-mandelate. However, these experiments did not reveal the chemical identity of the pair of acid/base catalysts, nor did they allow these catalysts to be associated with specific residues in the known amino acid sequence of the enzyme (Ransom et al., 1988).

The structure of the active site of MR is also of considerable interest since this enzyme appears to be nonstereospecific with respect to its enantiomeric substrates. The values for V_{max} and K_m in both the (*R*) to (*S*) and the (*S*) to (*R*) directions are, within error, identical (Whitman et al., 1985). In addition, the pH dependence of k_{cat} reveals two ionizable groups with pK_as of 6.4 and 10.0 in both directions, with the basic form of one group and the acidic form of the second group being required for catalysis in both directions (Landro et al., 1991). This kinetic symmetry is especially interesting since the experiments described in the previous paper suggest that the acid/base functional groups are chemically inequivalent. Therefore, MR provides an interesting contrast to the situation thought to apply in the reaction catalyzed by proline racemase in which a single active site is presumed to be located at the interface of two identical polypeptides in the dimeric enzyme (Rudnick & Abeles, 1975). Both chemical modification experiments (Rudnick & Abeles, 1975) and measurements of the fractionation factors of the active site acid/base catalysts (Belasco et al., 1986) suggest that these are thiols of two equivalent cysteine residues, one associated with each polypeptide chain. However, no structure has heretofore been reported for any racemase, including proline racemase.

The structural studies described herein permit the identification of likely catalytic residues in the active site of MR, including the two acid/base catalysts, and also establish the general disposition of the substrate in the active site. We have previously reported two crystal forms of MR (Neidhart et al., 1988); however, the crystal structure of the enzyme has now been solved with use of a newly discovered crystal form that diffracts to high resolution (<2.0 Å) and contains a single subunit of MR in the asymmetric unit. We report the conditions used to prepare this crystal form and the methods used to solve the X-ray crystal structure by multiple isomorphous replacement at 3.0-Å resolution. We also describe the refinement of the crystal structure at 2.5-Å resolution using both the simulated annealing refinement protocol of Brünger et al. (1987) (program XPLOR) and the restrained least-squares procedure of Hendrickson and Konnert (1980) (program PROLSQ). The combined application of these techniques together with manual rebuilding of the model, has produced a 2.5-Å resolution crystal structure with an *R*-factor of 18% and excellent conformity with ideal polypeptide geometry. A preliminary account of the structure of MR in the context of its homology with that of muconate lactonizing enzyme (MLE) has been reported (Neidhart et al., 1990).

Materials and Methods

Crystallization. Homogeneous MR from *Pseudomonas putida* was isolated according to published procedures (Tsou et al., 1989). For crystallization, the enzyme was concentrated to 40 mg/mL in a buffer composed of 50 mM Tris, pH 8.0, containing 10 mM $MgCl_2$ and 0.01% NaN_3. Crystals of MR were grown by hanging drop vapor diffusion against 30% saturated aqueous ammonium sulfate with use of the following procedure: first, a 5-μL drop of enzyme solution (40 mg/mL in the above buffer) was pipetted onto a silanized glass cover slip. The drop was diluted 2-fold by addition of 5 μL of distilled, deionized water and then mixed with 10 μL of a 30% saturated solution of ammonium sulfate in distilled, deionized water. The drop was then equilibrated at room temperature (about 20 °C) against 1 mL of 30% saturated ammonium sulfate in a standard hanging drop vapor diffusion format (McPherson, 1982) using Linbro 24-well tissue culture plates. Large, well-ordered crystals appeared overnight and were fully grown within one week. The crystals are stable in the crystallization drops for several months at room temperature. For diffraction analysis, crystals were mounted in quartz capillaries (Charles Supper Co., Natick, MA) sealed with mineral oil. For derivative screening and final data collection, crystals were transferred before mounting to a synthetic mother liquor composed of 40% saturated ammonium sulfate, 50 mM MES, pH 6.0, and 5 mM $MgCl_2$. Crystals cracked or dissolved upon transfer to mother liquors buffered at pH values above 6.0.

Characterization. Fifteen-degree precession photographs of the *h*0*l*, *hk*0, and *hk*1 zones of MR crystals were recorded on Kodak DEF film. The Laue symmetry of the crystals is *4/mmm*, and all reflections for which $h + k + l$ is odd are systematically absent. Since no other extinctions are apparent, this uniquely identifies the space group as I422 (Hahn, 1985). The unit-cell dimensions at 20 °C are $a = b = 125.0$ Å, $c = 106.2$ Å (±0.1 Å on each dimension); the dimensions change by less than 0.5% to $a = b = 124.5$ Å and $c = 106.2$ Å upon cooling to 5 °C (Table I). Diffraction spots are observed to about 2.0-Å resolution on still photos. Given the known

Table II: Derivatization Trials[a]

reagent	soaking conditions	result
$EuCl_3$	5 mM, overnight	intensity changes[b]
$PtCl_4^{2-}$	1 mM, overnight	severe cracking
$PtCl_4^{2-}$	1 mM, 2 h	mild cracking, intensity changes
$Pt(NH_3)_2Cl_2$	1 mM, overnight	intensity changes[b]
PIP	1 mM, overnight	strong intensity changes[b]
$HgCl_2$	0.5 mM, 2 h	mild cracking, strong intensity changes
$HgCl_2$	0.5 mM, 0.5 h	strong intensity changes[b]
$UO_2(OAc)_2$	1 mM, overnight	crystals destroyed
$K_3UO_2F_5$	1 mM, overnight	mild cracking, strong intensity changes

[a] All trials were performed either in unbuffered 40% saturated ammonium sulfate or in a synthetic mother liquor composed of 50 mM MES, pH 6.0, 40% saturated ammonium sulfate. $MgCl_2$ (5 mM) was also present in all soaks except those with uranyl or lanthanide reagents. PIP and uranyl solutions were prepared fresh. [b] Conditions used for high-resolution data collection.

subunit molecular mass of 38 570 daltons (Ransom et al., 1988), assumption of one subunit as the contents of the asymmetric unit leads to a calculated V_m of 2.7 Å^3/dalton, a value well within the observed range of 1.8–3.5 as compiled by Matthews (1968).

Derivative Search. MR crystals were tested for reaction with heavy atom reagents by soaking the crystals in dilute solutions of the reagent in either unbuffered 40% saturated ammonium sulfate or the synthetic mother liquor described above. Crystals that remained intact were surveyed by precession photography for changes in the relative intensities of diffraction spots as compared with native photographs. The results of the preliminary derivative search are summarized in Table II. Low-resolution (5.0-Å) data sets were collected from native MR crystals and from promising derivatives for further assessment of the quality of the derivatives.

Data Collection. All diffraction data from crystals of MR were measured with use of a Nicolet P3 single crystal diffractometer. The X-ray source was an AEG/Telefunken sealed copper target X-ray tube operated at an accelerating potential of 50 kV and a current of 30 mA. Typical crystals of MR used for data collection had dimensions of about 1.0 mm × 0.6 mm × 0.4 mm, so the source colimator was adjusted to produce an incident X-ray beam about 1.0 mm in diameter at the crystal. The crystal to detector distance was about 500 mm and a thin nickel filter was used to reduce K_β spectral contamination. Because of the systematic extinction of adjacent reflections produced by body centering and the small mosaic spread of the crystals, diffraction spots were well resolved with this arrangement. With the exception of the native ∞–5.0-Å shell, all data sets were collected at reduced temperature to minimize radiation damage. An open stream of chilled nitrogen from a modified Nicolet LT-1 low-temperature device was used to maintain the crystals at a temperature between 0 and 5 °C during data collection. Under these conditions the crystals had a useful lifetime in the X-ray beam of about 60 h, as compared with 20 h at room temperature.

All diffraction data were measured by use of full-width ω scans in background–peak–background mode. About 1 min was spent on each reflection, with 40 s devoted to scanning the peak. Typical peak widths were about 0.5°. The Friedel pairs collected for derivative data were true Friedels rather than Bijvoet pairs, in order to minimize differences in absorption. The empirical procedure of North et al. (1968) was used to correct the intensities for absorption effects. A linear decay correction was applied on the basis of least-squares analysis of a set of five check reflections monitored during data collection. Final data reduction and all subsequent processing was accomplished using the PROTSYS package of protein crystallographic programs (available upon request from G. A. Petsko).

Structure Solution at 5.0-Å Resolution. Diffraction data were collected to 5.0-Å resolution from a native MR crystal and from crystals derivatized with $EuCl_3$ and with $Pt(NH_3)_2Cl_2$. Each data set was measured by use of a single crystal, and derivative data sets included Friedel pairs. Statistics on the data collection are included in Table I. Isomorphous difference Patterson maps were calculated and were interpreted both manually and by use of the computer program HASSP (Terwilliger et al., 1987). Each derivative was cleanly interpretable in terms of a single major metal binding site per asymmetric unit. The positions and occupancies of these sites were refined by the method of origin-removed Patterson correlation using the computer program HEAVY by Terwilliger and Eisenberg (1983). Since *B*-factors are indeterminate in low-resolution analysis, they were fixed at 15.0 Å^2 for each derivative. Preliminary phases for native structure factors were then calculated by the method of Blow and Crick (1959) with use of only the europium isomorphous differences and also by the method of Blow and Crick as modified by North (1965) and Matthews (1966) including the anomalous differences for the europium derivative with both their original and opposite sign. Cross-difference Fourier maps were then calculated with use of the platinum isomorphous differences and each of these three sets of phases on the basis of the europium SIR and SAS data. Comparison of the maximal peak heights in these Fourier maps revealed that the original sign of the anomalous differences degraded the phasing, whereas the opposite sign enhanced it (as judged by the signal to noise ratio of peaks in resulting difference Fourier maps). Thus, the signs of the coordinates of the europium site were reversed in order to convert the crystal structure to the correct enantiomorph. The position of the platinum site was then assigned on the basis of a cross-difference Fourier map calculated by use of platinum isomorphous differences and SIRSAS phases from the europium derivative. The positions for both derivatives were checked against the isomorphous difference Patterson maps and were then subjected to a final round of difference Patterson refinement. "Best" MIR phases for native structure factors were calculated by use of these refined derivative positions and occupancies and both isomorphous and anomalous differences for the europium and platinum derivatives. Lack of closure residuals (*E*-values) were calculated in shells of resolution for acentric reflections, and the anomalous *E*-values were set to one-third of the value of the overall isomorphous *E*-value. The final phase set had an overall figure of merit of 0.72 and was used to calculate a native Fourier synthesis at 5.0-Å resolution. This protein electron density map clearly revealed the packing of MR in the unit cell and displayed a number of rods of density that could be interpreted as α-helices.

Extension to Higher Resolution. In principle, it might have been possible to solve the crystal structure of MR at high resolution using only the two derivatives that had proved successful in the low-resolution studies; however, the mean fractional isomorphous difference for each derivative was on the order of 10–13% on $|F|$, a relatively small value that could easily be swamped out by error in measuring the weaker high-resolution data. Thus, additional derivatives with greater heavy atom substitution were sought in order to increase the heavy atom contribution.

Final Derivative Screening. Since a platinum derivative had already been successfully prepared, the diplatinum reagent PIP [bis(μ-iodobis(ethylenediamine)diplatinum(II) nitrate;

Table III: Refined Heavy Atom Coordinates[a]

derivative	x	y	z	occupancy[b]	B (Å²)
$EuCl_2$	26.77	4.11	17.31	0.145	28
	15.81	5.60	10.30	0.067	80
$Pt(NH_3)_2Cl_2$	37.97	14.44	−13.17	0.155	85
PIP	37.97	15.56	−12.95	0.157	20
	40.58	8.09	−12.00	0.131	20
$HgCl_2$	26.89	4.85	−10.83	0.102	14
	15.81	6.60	11.46	0.133	26

[a] Heavy atom sites were located by difference Patterson and difference Fourier methods and refined by the method of origin-removed difference Patterson correlation (Terwilliger & Eisenberg, 1983). The coordinates are listed in orthogonal angstrom units. [b] Occupancy in arbitrary units.

STREM Chemical Co., St Louis, MO] offered the possibility of preparing an additional platinum reagent with a greater concentration of electrons. The use of this compound for crystallographic studies was first described in relation to the solution of the 7-Å resolution crystal structure of the nucleosome core particle (O'Halloran et al., 1987). The mode of binding of this compound to macromolecules was then unknown; however, the 3-Å resolution crystal structure of MR reveals that PIP binds to methionine residues and has probably dissociated into separate platinum ions upon binding. PIP produced striking intensity changes upon soaking with crystals of MR and provided one of the best derivatives. In addition, MR contains two cysteine residues (Ransom et al., 1988), only one of which is reactive toward DTNB under nondenaturing conditions (Powers, 1989). Thus, small, amphipathic mercurial reagents were screened that might bind to both cysteine sulfhydryls without disrupting the protein structure; mercuric chloride produced very strong intensity changes upon soaking for only half an hour with MR crystals. A summary of the heavy atom reagents screened for reaction with crystals of MR appears in Table II.

Structure Solution at 3.0-Å Resolution. Final data collection on native and derivatized crystals of MR typically required several crystals per data set, so the derivative data were collected in overlapping shells of increasing resolution (decreasing d_{min}). Merging of the different shells of data constituting a complete data set was accomplished with use of the computer program SSM, which calculates and applies scale factors according to the method of Fox and Holmes (1967). The merging R-factors for overlapping reflections are typically about 6% on intensity (Table I). SSM was also used to ensure that the hand of the anomalous scattering was consistent among different crystals used for a derivative data set. Anomalous differences were further analyzed and corrected for systematic errors by scaling the average ratio between F^+ and F^- to 1.0 in blocks of reciprocal space (North et al., 1968). The derivative data sets were then scaled in blocks of reciprocal space to the native data.

The europium and platinum derivatives were checked and refined against the difference Pattersons at their limiting resolutions and were used to calculate "best" MIR phases at 3.5-Å resolution. Isomorphous difference Fourier analysis of the PIP and $HgCl_2$ derivatives revealed two unique binding sites for each derivative. Since the binding sites for PIP were only 8 Å apart, and the mode of binding of PIP to macromolecules was unknown (O'Halloran et al., 1987), the PIP derivative was modeled as two independent Pt^{2+} ions, one at each site. A final round of isomorphous difference Fourier analysis at 3.0 Å revealed a minor europium binding site, which was then refined by difference Patterson methods. A summary of all data collection performed on MR crystals appears in Table I, and final refined heavy atom parameters are listed in Table III. The mean fractional isomorphous differences for the derivatives are 12%, 10%, 16%, and 17% for the $EuCl_3$, $Pt(NH_3)_2Cl_2$, PIP and $HgCl_2$ derivatives, respectively.

A 3.0-Å MIR phase set was calculated with use of all available derivative data; however, resulting isomorphous difference Fourier maps contained peculiar streaks around heavy atom positions that were traced to poor phasing in the 3.5–3.0-Å shell. Only the mercury derivative contributes strongly to the phasing in the 3.5–3.0-Å shell (Table IV), so the reflections in this shell are effectively SIR phased and hence are ambiguous. Phase improvement by solvent flattening, back transformation, and recombination of the back-transformed phases with the original MIR phase probability distributions provided a resolution of these phase ambiguities (Wang, 1985; de Vos et al., 1988) and facilitated production of an interpretable electron density map of MR at 3.0-Å resolution. A solvent content of 50% was assumed for the crystals on the basis of their calculated V_m of 2.7 Å³/dalton (Matthews, 1968), a molecular envelope was calculated from the preliminary 3.0-Å MIR electron density map, and five cycles of solvent flattening, back-transformation, and phase recombination were performed. A second molecular envelope was calculated followed by additional cycles of solvent flattening, but no further improvement was realized in the figure of merit or the appearance of calculated electron density maps. The final set of phases produced by application of solvent

Table IV: MIR Phasing Statistics for Mandelate Racemase[a]

	resolution (Å)										
	9.4	6.7	5.5	4.7	4.2	3.9	3.6	3.3	3.15	3.0	total
native											
FOM[b]	0.92	0.87	0.78	0.74	0.70	0.66	0.64	0.50	0.47	0.44	0.64
no.	285	449	502	649	716	783	776	804	720	605	
Eu^{3+}											
F_H/E[c]	1.93	1.84	1.71	1.76	1.36	1.15	0.97	0.87	0.77	0.72	1.22
no.	284	440	478	633	697	745	764	774	677	567	
$Pt(NH_3)_2Cl_2$											
F_H/E	2.23	1.96	1.40	1.22	0.88	0.69					1.32
no.	281	442	482	615	637	374					
PIP											
F_H/E	1.69	2.44	2.20	1.89	1.67	1.71	1.69	1.60			1.85
no.	282	427	454	589	665	729	702	229			
$HgCl_2$											
F_H/E	2.66	2.56	2.17	1.74	1.38	1.16	1.35	1.38	1.34	1.41	1.62
no.	276	411	429	552	636	661	626	522	546	398	

[a] Phases for native structure factors were calculated with use of the PRPTSYS suite of crystallographic programs. [b] FOM is the average figure of merit. [c] F_H/E is the ratio of the calculated heavy atom contribution to the root mean square lack of closure error and is a measure of phasing power of the derivative.

flattening had an overall figure of merit of 0.85 at 3.0-Å resolution.

Chain Tracing. A 3.0-Å resolution electron density map of MR was calculated and transferred to a "minimap" of stacked transparencies. The envelope of a single subunit and the major secondary structural features of MR were identified. Tentative positions for C_α atoms of the polypeptide backbone were defined at intervals of approximately 3.8 Å and were entered along with the electron density map into the macromolecular display and modeling program FRODO (Jones, 1985) running on an Evans and Sutherland PS330 vector graphics system. Additional C_α positions were defined both within FRODO and on the minimap. The characteristic topologies of a parallel α/β-barrel (Banner et al., 1975) and an antiparallel β-sheet were identified.

Once most of the 358 C_α atoms in MR were identified, the tentative C_α positions were rationalized with the known amino acid sequence (Ransom et al., 1988). The mercury binding sites were used as markers for the positions of the cysteine side chains, and the positions of the surrounding tentative C_α positions were sequentially renumbered and adjusted to achieve correspondence between the sequence and the electron density for side chains apparent in the map. The distances between adjacent C_α atoms were also adjusted to the stereochemically reasonable value of 3.8 Å.

Construction of a Complete Atomic Model. To expedite construction of a complete atomic model, the fragment fitting option ".FRGL" (Finzel et al., 1990) in FRODO was used to build a polyalanine backbone from the C_α coordinates. The geometry regularization option in FRODO was used to idealize the geometry between fitted fragments. Side chains were added to the atomic model by substituting the correct sequence for the polyalanine backbone, calculating idealized coordinates, and moving the side-chain atoms into electron density by use of the various modeling capabilities of FRODO.

Refinement. The complete preliminary atomic model of MR was initially subjected to molecular dynamics refinement against the experimental X-ray structure factor magnitudes at 3.0-Å resolution with use of the computer program XPLOR (Brünger et al., 1987). An initial energy refinement (energy minimization with an energy term related to the difference between observed and calculated structure factor magnitudes) reduced the *R*-factor from 43 to 26%. Random velocities were then imparted to the atomic coordinates to produce an average kinetic energy equivalent to that expected at 4000 K, and the system was allowed to equilibrate for 1000 time steps of 1 fs. An additional 2000 steps (2 ps) of slow cooling (velocity rescaling every 25 time steps) from 4000 to 300 K, followed by energy refinement, reduced the *R*-factor to 20% while good polypeptide geometry was maintained. Further refinement against experimental diffraction data to 2.5-Å resolution was performed with use of both energy refinement in XPLOR and the restrained parameter least-squares procedure of Hendrickson and Konnert (1980) (program PROLSQ). Manual rebuilding of the atomic model between cycles was essential to the progress of the refinement when either of these protocols was used.

Identification of the Active Site. In order to locate the divalent metal ion binding site, a crystal grown in the presence of Mg^{2+} was transferred to a 10 mM solution of Mn^{2+} in 50 mM MES, pH 6.0/30% saturated ammonium sulfate. Diffraction data were collected to 5.0-Å resolution, and an isomorphous difference Fourier map was calculated by use of phases calculated from the refined model. In a separate experiment, native (i.e., with Mg^{2+} as cofactor) crystals were transferred to a solution containing 5 mM (*R,S*)-*p*-iodomandelate in the standard synthetic mother liquor. Diffraction data for this complex were collected to 3.5 Å as described above, and isomorphous difference maps were calculated by use of refined phases and either native or calculated structure factor magnitudes.

Synthesis of (R,S)-p-Iodomandelate. *p*-Iodomandelic acid was synthesized from NaCN and *p*-iodobenzaldehyde (Karl Industries, Inc.) as described for the synthesis of mandelic acid by Maggio et al. (1975). A 55% yield was obtained after two recrystallizations from hot water: mp 138–139 °C. Anal. Calcd: C, 34.54; H, 2.54; I, 45.66. Found: C, 34.67; H, 2.56; I, 45.81. NMR at 240 MHz (DMSO-d_6): δ 5.05 (1 H, s), 7.25 (2 H, d, J = 8.1 Hz), 7.74 (2 H, d, J = 8.1 Hz).

Results and Discussion

Refinement. The crystallographic residual between structure factor magnitudes calculated from the preliminary atomic model and those observed experimentally to 3.0-Å resolution was 43%. Refinement using molecular dynamics and energy refinement in XPLOR rapidly reduced the *R*-factor to 20% for all observed data between 10.0- and 3.0-Å resolution.

The only large-scale rearrangements of the polypeptide chain observed in the course of this refinement occurred in the region of a mobile loop connecting the first two strands of the N-terminal β-meander. Much of this loop was not apparent in the improved MIR electron density map, and the initial model was constructed arbitrarily. Simulated annealing refinement at 3.0-Å resolution revealed no significant electron density for the distal portion of the loop composed of residues 19–30, so these residues were omitted from all subsequent calculations.

Additional refinement at 2.5-Å resolution was performed by use of the restrained least-squares method (program PROLSQ; Hendrickson & Konnert, 1980). In the course of this refinement, it was deemed necessary to shift the polypeptide chain of the first helix in the central β-barrel by one residue in order to account for the side-chain density of Arg 151. This shift was accommodated by rebuilding of the connecting loops at either end of the helix, and no other major revisions to the main chain were necessary. Also during this refinement, a persistent lobe of electron density in the active site was interpreted as a sulfate ion, and the corresponding coordinates were added to the atomic model (see below). The *R*-factor is now 18.3% for all data greater than $1\sigma(F)$ from 5.0–2.5-Å resolution (8992 reflections or 70% of those possible); the root mean square deviation from ideality of bond distances is 0.015 Å and for 1–3 angle distances is 0.053 Å. Further refinement against diffraction data to 2.0-Å resolution is in progress.

The Polypeptide Fold. The major secondary structural features of MR are outlined in Table V. Conceptually, the polypeptide fold can be dissected into three distinct domains. Stereodiagrams of the polypeptide backbones of the three domains are presented in Figure 1, and a stereoview of the entire backbone is presented in Figure 2. The N-terminal domain has an $\alpha + \beta$ architecture composed of a three-stranded antiparallel β-sheet commonly called a β-meander (Schulz, 1980) and an antiparallel four-α-helix bundle (Richardson, 1981) (Figure 1A). This domain is connected by a long stretch of extended β-type structure to the first β-strand of an eight-stranded singly wound parallel α/β-barrel. This central β-barrel domain (Figure 1B) is similar to the barrel topology observed first in triose phosphate isomerase (Banner et al., 1975) and subsequently in a number of other enzymes, except for one feature: most parallel β-barrels have eight strands of β-sheet and eight major α-helices connected consecutively +1×, +1×... (Richardson, 1981) to form a

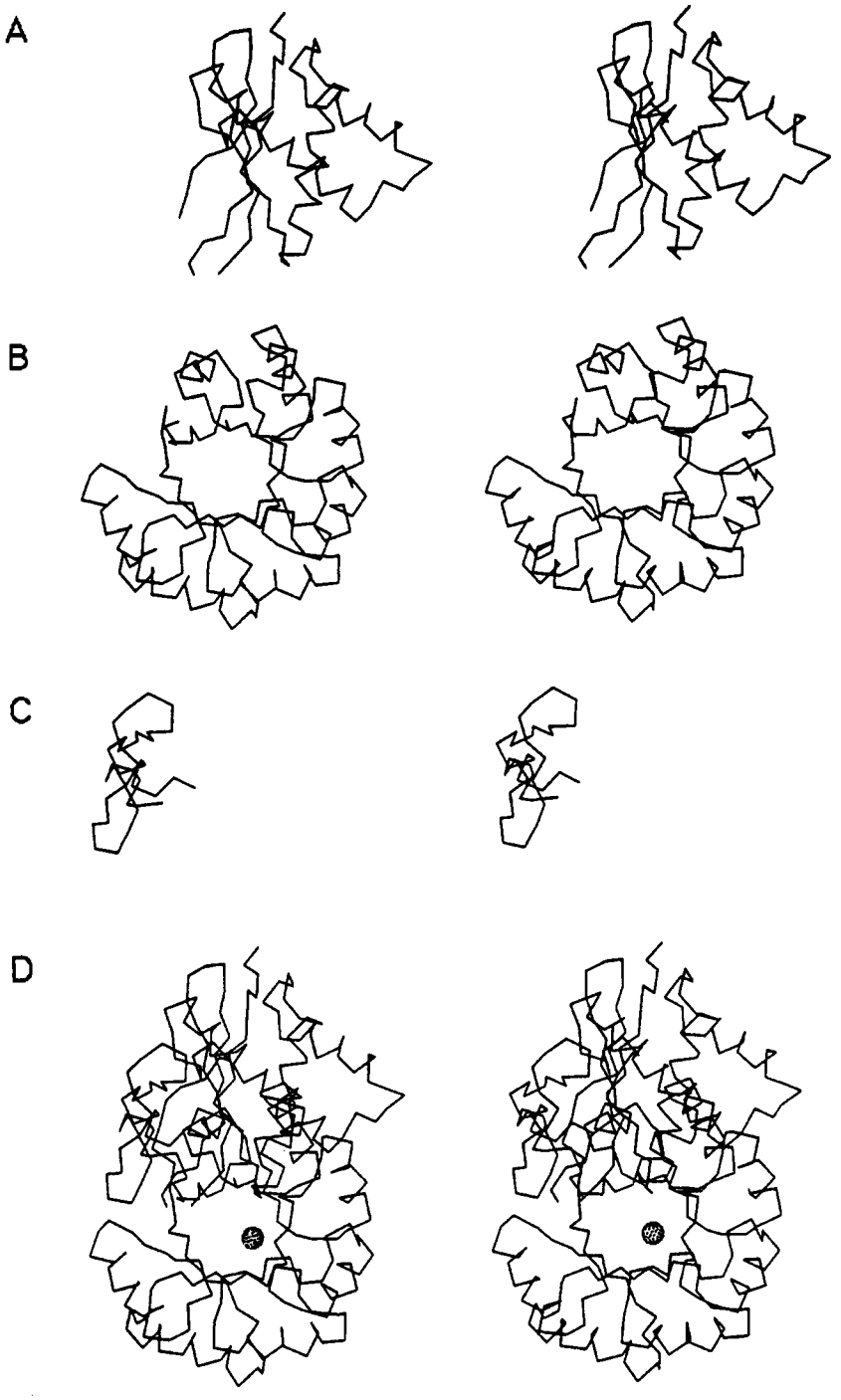

FIGURE 1: Stereo backbone tracings of the three domains of MR from the same perspective: (A) the N-terminal $\alpha + \beta$ domain; (B) the central parallel β-barrel; (C) the irregular C-terminal domain; (D) the intact subunit.

structure with *pseudo* 8-fold rotational symmetry. In MR the eighth α-helix is absent from the barrel; an irregular C-terminal domain composed mostly of extended strands (Figure 1C) serves to fill much of the space normally occupied by this eighth α-helix in other β-barrel structures. In addition to the "major" helices of the central β-barrel, a single turn of α-helix is present in the loop between the sixth strand (β9) and the sixth "major" α-helix of the barrel (αJ); we denote this intervening feature as helix αJ'.

To date, 17 enzymes have been shown to possess a parallel α/β-barrel domain structure (Farber & Petsko, 1990), yet relatively few general principles have emerged. Like MR, all parallel α/β-barrels have eight core strands of β-sheet, and the active site is always located near the mouth of the barrel at the C-terminal end of the core β-strands (see below). Also, in all known parallel α/β-barrels the β-strands are tilted by about 35° relative to the barrel axis, with the helices running roughly parallel to the strands, and the "shear number" is 8, corresponding to an offset of one residue between each strand of the core β-sheet (McLachlan, 1979). On the basis of analysis of three α/β-barrels, Lesk et al. (1989) have suggested that the α/β-barrel domains could be divided into two distinct classes on the basis of the packing arrangement of side chains in the central core of the barrel. However, the core of MR does not seem to conform to either of their proposed classes, suggesting that a two-class system may be too simple.

Quaternary Structure. Mandelate racemase is revealed by the crystal structure to be tightly packed as an octamer of identical subunits (subunit mass 38.4 kDa) related by 422 (D_4) point symmetry. This quaternary structure has also been

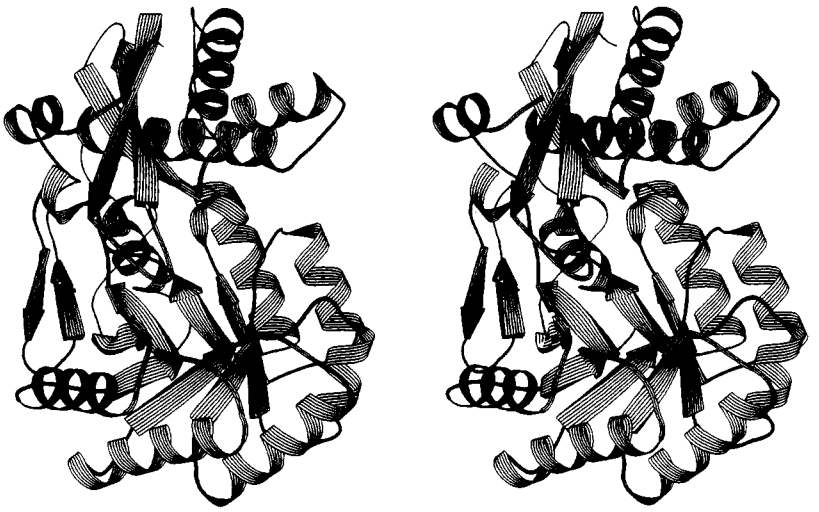

FIGURE 2: Stereo "cartoon" of the polypeptide fold of MR, produced with the computer program RIBBON (Priestle, 1988). β-Sheet strands are represented as arrows, α-helices as coiled ribbons, and irregular structure as tubes. The N-terminal domain is at the top of the figure.

Table V: Secondary Structure Elements

domain	2° structure	residues
N-terminus		
antiparallel β-meander	β1	5–16
	β2	32–41
	β3	46–52
antiparallel α-helix bundle	αA	56–73
	αB	80–90
	αC	98–117
	αD	123–126
Central		
parallel α/β-barrel	β4	134–139
	αE	148–157
	β5	162–166
	αF	172–186
	β6	191–195
	αG	202–213
	β7	220–221
	αH	229–236
	β8	243–245
	αI	251–260
	β9	266–267
	αI′	271–274
	αJ	276–289
	β10	293–297
	αK	300–307
	β11	313–319
C-terminus		
	β12	331–333
	β13	336–338
	αL	351–354

described in hemerythrin (Stenkamp & Jensen, 1981), glycolate oxidase (Lindqvist & Brändén, 1985), and MLE (Goldman et al., 1985). One of the interfaces between 2-fold related subunits is more intimate than the 4-fold interfaces, so the structure is best described as a tetramer of dimers (as opposed to a dimer of tetramers). Further evidence for a tight dimer interface in MR is provided by the observation that residues from a 2-fold related subunit form part of the active site (see below). Our observation of an apparent tight dimer in MR is consistent with the hypothesis that proteins composed of $2n$ identical subunits are assembled as n-mers of dimers (Miller, 1989). In addition, failure of tight dimers to dissociate under the conditions of SDS–PAGE may account for the MR subunit molecular mass of about 70 000 daltons that was proposed earlier by Fee et al. (1974a) and their conclusion that the enzyme is tetrameric in solution.

The subunits of MR are oriented in the octamer so that the pseudorotational axis of the β-barrel is perpendicular to the 4-fold axis of the 422 octamer and roughly tangent to the sphere defined by the globular octamer. Helix αA packs antiparallel with its congener in a 2-fold related subunit, and an additional symmetrical contact within the putative tight dimer is provided by the loop connecting αB and αC. Thus, much of the tight dimer interface is provided by the N-terminal domain of MR (Figure 3) with additional contact being made at connecting loops of the central β-barrel at the C-terminal ends of β7 and β8. The 4-fold contacts between dimers occur mostly at loops on the N-terminal ends of β8, β9, and β10 and at the C-termini of β6 and β7. The orientation of the MR subunit in the octamer is identical with that observed for MLE (Goldman et al., 1985), and the general nature of the subunit contacts appears to be conserved, lending strength to the notion that these two enzymes evolved from a common precursor (Neidhart et al., 1990).

The Active Site. The location of the active site of MR has been established by observing crystallographically the binding of several ligands. Europium(III) ion is known to substitute for divalent metal ions at specific binding sites in proteins (Horrocks, 1982), and the major Eu^{3+} binding site was assumed to define the position of the catalytic metal ion in the native enzyme. This assumption was confirmed by performing a difference Fourier analysis at 5.0-Å resolution of diffraction data from MR crystals soaked in the presence of excess $MnCl_2$. Unlike europium, which strongly inhibits MR (Powers, 1989), manganese is known to activate the enzyme (Fee et al., 1974). This substitution of manganese ion for magnesium ion corresponds to a net change of 13 electrons and produced a single major difference electron density peak with maximal value greater than 10 times the estimated standard deviation in the map. The position of this peak, the position of the refined derivative europium ion, and the refined position of the magnesium ion in the native structure all agree to within 0.5 Å. The metal ion is ligated by three carboxyl groups contributed by the side chains of Asp 195, Glu 221, and Glu 247 (Figure 4). These residues are located at the C-terminal ends of the third, fourth, and fifth β-strands of the central α/β-barrel domain.

Further confirmation of the location of the active site and the general disposition of bound substrate were revealed by difference Fourier analysis at 3.5-Å resolution of diffraction data from a crystal of MR soaked in mother liquor containing 5 mM (*R,S*)-*p*-iodomandelic acid. *p*-Iodomandelate is a substrate for MR (R. Li and G. L. Kenyon, unpublished ob-

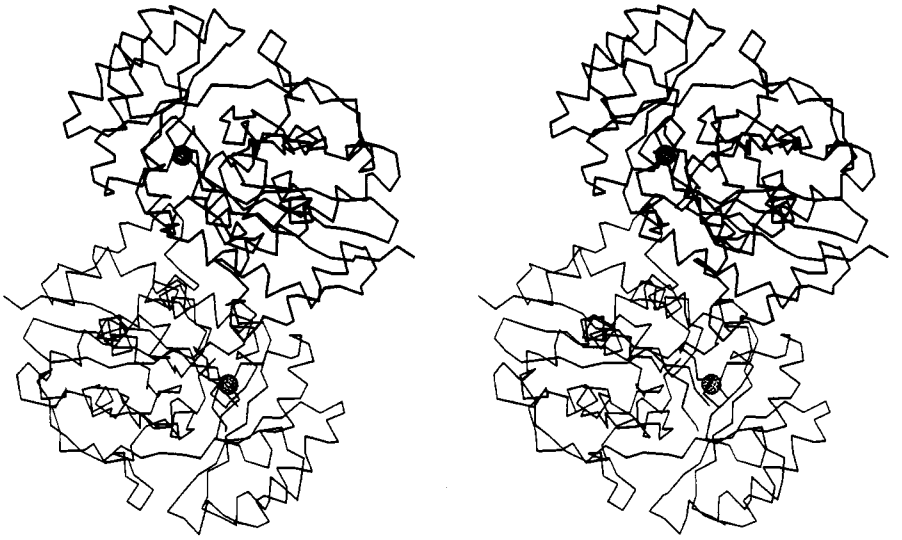

FIGURE 3: A tight "dimer" interface in MR. Two subunits related by the symmetry operation $[x',y',z'] = [x,-y,-z]$ are illustrated as backbone tracings (one backbone is shown with a light line and the second is shown with a dark line). The catalytic metal ions are represented as stipled spheres.

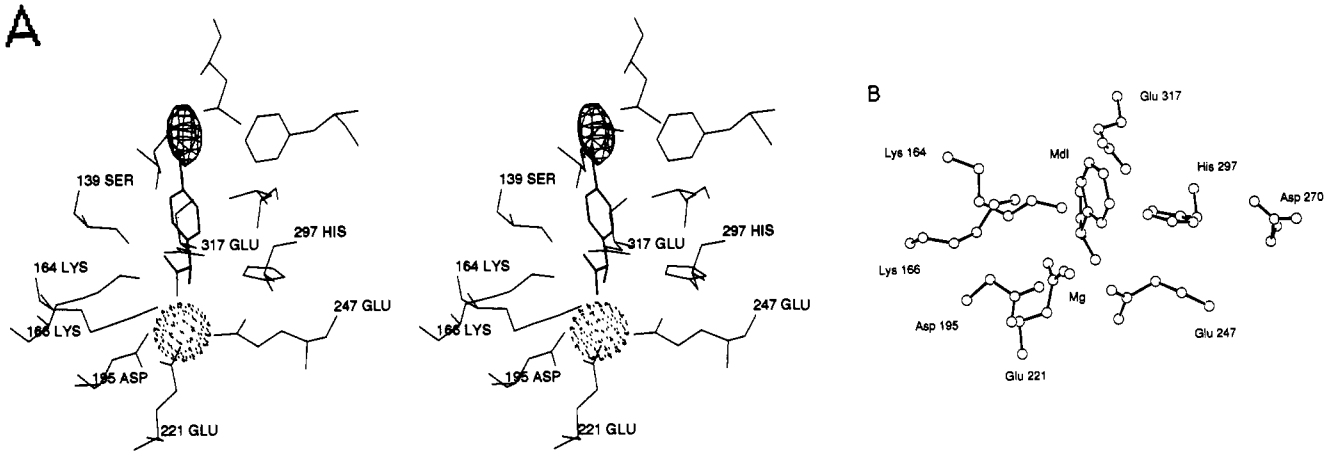

FIGURE 4: Models of the MR active site with complexed substrates. (A) The 2.5-Å refined atomic model of MR is shown in stereo, along with the major peak in the 3.5-Å *p*-iodomandelate difference Fourier map, contoured at 5σ. Phases for the electron density map were calculated from the refined atomic model of the native enzyme with the sulfate ion omitted. A model of *p*-iodomandelate bound to the enzyme is shown in bold lines. Only the iodine atom is clearly visible in the difference electron density map for the complex, so the model was initially placed by assuming that the bound sulfate ion in the native structure defines the position of the carboxyl group of substrate in the Michaelis complex. The model was then subjected to energy minimization in CHARMM (Polygen, Inc.) with the enzyme structure held fixed. The resulting model is in agreement with the experimentally observed locations of the anion binding site and the iodine substituent. (B) An ORTEP diagram of the modeled position of (*S*)-mandelate and the principal active site residues.

servations), and the electron-dense iodine substituent greatly aided efforts to locate substrate at moderate resolution (Figure 4A).

The active site of MR is located in the mouth of the central β-barrel, at the C-terminal end of the core β-strands. This is the location of the active site in all known parallel α/β-barrel enzymes (Chothia, 1988). It is also generally true that in multidomain and multisubunit enzymes the active sites lie at interfaces between domains and/or subunits (Schulz & Schirmer, 1979); the active site of MR is located at the interface between the N-terminal domain and the central β-barrel and also contains residues from a 2-fold related subunit in the octamer. However, despite the participation of more than one subunit in forming the active site, the crystal structure reveals eight independent active sites per octamer; the active site does not lie at a point of symmetry as is believed to be the case in proline racemase (Rudnick & Abeles, 1975; Belasco et al., 1986).

The residues that appear to be directly involved in substrate binding or catalysis are listed in Table VI. The major features of the active site are a hydrophobic pocket for the phenyl substituent of substrate, a binding site for the catalytically essential metal ion, and several charged residues that may be involved in catalysis. Like the metal binding residues, all of the residues that are likely to be involved in catalysis are contributed by the core β-strands of the central α/β-barrel. Conversely, the binding site for the phenyl substituent is composed of residues from both major domains and probably includes residues of the mobile "flap" composed of residues 19–30.

In addition to the electron density for the protein side chains,

Table VI: Active Site Residues

ligands to active site metal ion	Asp 195	hydrophobic pocket	Leu 18
	Glu 221		Val 22
	Glu 247		Val 29
	sulfate ion		Phe 52
putative catalytic bases	His 297		Tyr 54
	Lys 166		Leu 93′[a]
other residues near the metal ion and bound sulfate	Ser 139		Leu 298
	Lys 164		Leu 319
			Leu 321

[a] Leu 93′ is contributed by a 2-fold related subunit.

a strong lobe of electron density appears immediately adjacent to the metal ion in the native electron density map and may be attributed to either a water molecule or a sulfate ion. This lobe of density is also within 4 Å of the side-chain carboxyl group of Glu 317, the ϵ-amino groups of Lys 164 and Lys 166, the hydroxyl group of Ser 139, and the imidazole group of His 297. Given the strength of this electron density feature, we propose that it is associated with a bound sulfate ion.

It is probable that this sulfate ion lies in an anion binding site that would be occupied by the carboxyl group of mandelate in the Michaelis complex. Furthermore, modeling studies suggest that coordination of the carboxylate group of the substrate with the essential metal ion is also consistent with the observed position of the iodine substituent of *p*-iodomandelate complexed with MR (Figure 4A). Constraining the carboxylate groups and phenyl rings of the enantiomers of mandelate to these positions reveals that the α-hydrogen of (*S*)-mandelate is accessible to the ϵ-amino group of Lys 166 and that the α-hydrogen of (*R*)-mandelate is accessible to the imidazole group of His 297. These assignments for the two acid/base catalysts in the active site of MR are in agreement with the suggestions made in the previous paper that the conjugate acid of the (*S*)-specific base is polyprotic and that the conjugate acid of the (*R*)-specific base is monoprotic. An ORTEP diagram of (*S*)-mandelate modeled in the active site is shown in Figure 4B.

Since the sulfate ion is directly ligated to the catalytic metal ion, this may indicate that the metal ion participates in stabilizing negative charge on the intermediate and associated transition states through polarization of the carboxyl group of substrate. It is likely that Lys 164 also participates by donating a proton to the substrate carboxyl group; however, additional experimental verification of the proposed binding mode will be required to confirm these roles.

The observed dependencies of k_{cat} on pH (Landro et al., 1991) are consistent with the participation of two functional groups having pK_as of 6.4 and 10.0 in both the (*R*) to (*S*) and (*S*) to (*R*) directions, assuming that these kinetically determined pK_a values are actually microscopic pK_a values for the functional groups in the active site (Knowles, 1976). The lower value (pK_a 6.4) is nominally consistent with the imidazole group of His 297 participating in catalysis as a general base in the (*R*) to (*S*) direction, but the primary amino group of Lys 166 must be strongly influenced by its environment to possess a pK_a value of this magnitude in the (*S*) to (*R*) direction. It is possible that the proximities of both the metal ion and the ϵ-amino (ammonium) group of Lys 164 destabilize the positive charge on Lys 166 and increase its acidity. Precedent for a dramatically reduced pK_a value for a lysine residue is provided by the work of Westheimer and co-workers on acetoacetate decarboxylase. In acetoacetate decarboxylase, an active site lysine forms an aldimine linkage with acetoacetate (Hamilton & Westheimer, 1959). Spectrophotometric titration of a reporter group incorporated into the active site by aldimine linkage to this lysine and comparison to the solution pK_a value of a model compound indicated a shift of about 4 pK_a units toward decreased basicity (Kokesh & Westheimer, 1971). This was confirmed by measuring the pH rate profile of acylation of the active site lysine with a different spectroscopic probe (Schmidt & Westheimer, 1971). It was proposed that this altered pK_a value was the result of the electrostatic environment of the active site and that this accounted for the ability of the active site lysine to function as a nucleophile at pH 6. Interestingly, sequencing of an active site peptide from acetoacetate decarboxylase demonstrated that the residue adjacent to the lysine that forms the aldimine linkage is also a lysine. Although the spatial disposition of these adjacent residues in acetoacetate decarboxylase is unknown, it was suggested that propinquity of these groups might be responsible for the apparent electrostatic destabilization of the associated positive charges. Since Lys 164, Lys 166, and the Mg^{2+} of MR have now been demonstrated to be close in space, a similar mechanism for reduction of the pK_a value of Lys 166 into the range useful for general basic catalysis at neutral pH may apply. His 297 is also in close proximity to the carboxylate groups of both Asp 270 and Glu 317; the negative electrostatic potential of these residues may effectively shield His 297 from the positive electrostatic potential associated with Lys 164 and Mg^{2+}, thereby allowing its pK_a value to appear "normal" when it is acting as the general basic catalyst. Thus, both Lys 166 and His 297 are viable candidates for general basic catalysts in MR.

The value of 10.0 observed for the pK_a of the acidic catalyst in both directions is consistent with the normal acidity of the ϵ-ammonium group of a lysine but is unusually high for the imidazole group of a histidine. As noted in the previous paragraph, the ionization properties of His 297 may now reflect a negative electrostatic environment. Perhaps the apparent increases in the pK_a values of both Lys 166 and His 297 when they function as general acidic rather than general basic catalysts either reflect a change in the distribution of charged residues in the active site or indicate that the kinetically determined pK_a values are not microscopic pK_a values for the ionizable groups (Knowles, 1976). In any event, the origin of this possible shift in pK_a values is of interest and is being explored by site-directed mutagenesis of pertinent active site residues.

The pK_a value of Lys 166 in the active site of the H297N mutant of MR is discussed in the following paper (Landro et al., 1991).

Conclusions. The results of this crystallographic study of MR have provided a partially refined model of the entire enzyme, with the exception of an extended loop that appears to be poorly ordered. The secondary, tertiary, and quaternary structures have been described and bear a striking resemblance to muconate lactonizing enzyme (Neidhart et al., 1990). These structural studies provide an unambiguous location for the active site, including the catalytically essential Mg^{2+}, and support the proposal that two acid/base catalysts are required for catalysis (Powers et al., 1991), with Lys 166 being the (*S*)-specific base and His 297 being the (*R*)-specific base. In the following paper in this issue (Landro et al., 1991), the mechanistic properties of the H297N mutant of MR are used to provide further evidence for the assignments of the two acid/base catalysts and to provide compelling evidence for a discrete *intermediate* in the racemization reaction.

Diffraction data on native crystals of MR have been collected to 2.0-Å resolution, and additional details of the active site geometry will be presented in the context of this fully refined structure. Other studies are also underway to better characterize the exact binding modes for enantiomeric substrates and to establish whether substantial rearrangement of the substrate and/or active site is involved in catalysis.

References

Banner, D. W., Bloomer, A. C., Petsko, G. A., Phillips, D. C., Pogson, C. I., & Wilson, I. A. (1975) *Nature 255*, 609.

Belasco, J. G., Bruice, T. W., Albery, W. J., & Knowles, J. R. (1986) *Biochemistry 25*, 2558.

Blow, D. M., & Crick, F. H. C. (1959) *Acta Crystallogr. 12*, 794–802.

Blundell, T. L., & Johnson, L. N. (1976) *Protein Crystallography*, Academic Press, NY.
Brünger, A. T., Kuriyan, J., & Karplus, M. (1987) *Science 235*, 458.
Chothia, C. (1988) *Nature 333*, 598.
Cooper, T. G. (1977) *The Tools of Biochemistry*, John Wiley and Sons, New York.
de Vos, A. M., Tong, Liang, Milburn, M. V., Matias, P. M., Jancarik, J., Noguchi, S., Nishimura, S., Miura, K., Ohtsuka, E., & Kim, S.-H. (1988) *Science 239*, 888.
Dodson, E., & Vijayan, M. (1971) *Acta Crystallogr. B27*, 2402.
Farber, G., & Petsko, G. A. (1990) *Trends Biochem. Sci. 15*, 228.
Fee, J. A., Hegeman, G. D., & Kenyon, G. L. (1974) *Biochemistry 13*, 2528.
Finzel, B. C., Kimatian, S., Ohlendorf, D. H., Wendoloski, J. J., Levitt, M., & Salemme, F. R. (1990) in *Crystallographic and Modeling Methods in Molecular Design* (Ealick, S., & Bugg, C., Eds.) pp 175–189, Springer-Verlag.
Fox, G. C., & Holmes, K. C. (1967) *Acta Crystallogr. 20*, 886.
Goldman, A. (1985) Ph.D. Thesis, Yale University.
Goldman, A., Ollis, D. L., & Steitz, T. A. (1987) *J. Mol. Biol. 194*, 143.
Hahn, T., Ed. (1985) *International Tables for X-ray Crystallography, Part A*, D. Reidel Publishing Co., Boston, MA.
Hamilton, G., & Westheimer, F. (1959) *J. Am. Chem. Soc. 81*, 6332.
Hendrickson, W. A., & Konnert, J. H. (1980) in *Biomolecular Structure, Function, Conformation and Evolution* (Srinivasan, R., Ed.) Vol. 1, pp 43–57, Pergamon, Oxford.
Horrocks, W. DeW. (1982) *Adv. Inorg. Biochem. 4*, 201.
Jones, T. A. (1985) *Methods Enzymol. 115*, 157.
Jones, T. A., & Thirup, S. (1986) *EMBO J. 5*, 819.
Kabsch, W., & Sander, C. (1983) *Biopolymers 22*, 2577.
Knowles, J. R. (1976) *CRC Crit. Rev. Biochem. 4*, 165.
Kokesh, F. C., & Westheimer, F. H. (1971) *J. Am. Chem. Soc. 93*, 7270.
Landro, J. A., Kallarakal, A. T., Ransom, S. C., Gerlt, J. A., Kozarich, J. W., Neidhart, D. J., & Kenyon, G. L. (1991) *Biochemistry* (third paper of three in this issue).
Lesk, A. M., Brändén, C.-I., & Chothia, C. (1989) *Proteins: Struct., Funct., Genet. 5*, 139–148.
Lindqvist, Y., & Brändén, C.-L. (1985) *Proc. Natl. Acad. Sci. U.S.A. 82*, 6855.
Maggio, E. T., Kenyon, G. L., Mildvan, A. S., & Hegeman, G. D. (1975) *Biochemistry 14*, 1131.
Matthews, B. W. (1966) *Acta Crystallogr. 20*, 230.
Matthews, B. W. (1968) *J. Mol. Biol. 33*, 491.
McLachlan, A. D. (1979) *J. Mol. Biol. 128*, 49.
McPherson, A. (1982) *The Preparation and Analysis of Protein Crystals*, John Wiley and Sons, New York.
Miller, S. (1989) *Protein Eng. 3*, 77.
Neidhart, D. J. (1989) Ph.D. Thesis, Massachusetts Institute of Technology.
Neidhart, D. J., Powers, V. M., Kenyon, G. L., Tsou, A. Y., Ransom, S. C., Gerlt, J. A., & Petsko, G. A. (1988) *J. Biol. Chem. 263*, 9268.
Neidhart, D. J., Kenyon, G. L., Gerlt, J. A., & Petsko, G. A. (1990) *Nature 347*, 692.
North, A. C. T. (1965) *Acta Crystallogr. 18*, 212.
North, A. C. T., Phillips, D. C., & Mathews, F. S. (1968) *Acta Crystallogr. A24*, 351.
O'Halloran, T. V., Lippard, S. J., Richmond, T. J., & Klug, A. (1987) *J. Mol. Biol. 194*, 705.
Powers, V. M. (1989) Ph.D. Thesis, University of California, San Francisco.
Powers, V. M., Koo, C. W., Kenyon, G. L., Gerlt, J. A., & Kozarich, J. W. (1991) *Biochemistry* (first paper of three in this issue).
Priestle, V. P. (1988) *J. Appl. Crystallogr. 21*, 572.
Ransom, S. G., Gerlt, J. A., Powers, V. M., & Kenyon, G. L. (1988) *Biochemistry 27*, 540.
Richardson, J. S. (1981) *Adv. Protein Chem. 34*, 167–339.
Rudnick, G., & Abeles, R. H. (1975) *Biochemistry 14*, 4515.
Schmidt, D., & Westheimer, F. (1971) *Biochemistry 10*, 1249.
Schulz, G. E. (1981) *Angew. Chem., Int. Ed. Engl. 20*, 143.
Schulz, G. E., & Schirmer, R. H. (1979) *Principles of Protein Structure*, Springer-Verlag, New York.
Stenkamp, R. E., & Jensen, L. H. (1981) in *Structural Aspects of Recognition and Assembly in Biological Molecules* (Balaban, M., Sussman, J. L., Traub, W., & Yonath, A., Eds.) Balaban ISS, Philadelphia.
Terwilliger, T. C., & Eisenberg, D. (1983) *Acta Crystallogr. A39*, 813.
Terwilliger, T. C., Kim, S.-H., & Eisenberg, D. (1987) *Acta Crystallogr. A43*, 1.
Tsou, A. Y., Ransom, S. R., Gerlt, J. A., Powers, V. M., & Kenyon, G. L. (1989) *Biochemistry 28*, 969.
Tsou, A. Y., Ransom, S. C., Gerlt, J. A., Buechter, D. D., Babbitt, P. C., Kenyon, G. L., & Kenyon, G. L. (1990) *Biochemistry 29*, 9856.
Wang, B. C. (1985) *Methods Enzymol. 115*, 90–111.